Carbohydrate Polymers 236 (2020) 115998

Contents lists available at ScienceDirect

Carbohydrate Polymers

journal homepage: www.elsevier.com/locate/carbpol

Photopolymerized Starchstarch Nanoparticle (SNP) network hydrogels

Michael J. Majcher[a], Carter L. McInnis[a], Sebastian Himbert[b], Richard J. Alsop[b], Dennis Kinio[c], Markus Bleuel[d], Maikel C. Rheinstädter[b], Niels M.B. Smeets[c], Todd Hoare[a,*]

[a] Department of Chemical Engineering, McMaster University, 1280 Main Street, West Hamilton, ON L8S 4L8, Canada
[b] Department of Physics and Astronomy, McMaster University, 1280 Main Street, West Hamilton, ON L8S 4L8, Canada
[c] EcoSynthetix Inc., 3365 Mainway, Burlington, ON L7M 1A6, Canada
[d] NIST Center for Neutron Research, National Institute of Standards and Technology, Gaithersburg, MD 20899-6100, United States

ARTICLE INFO

Keywords:
Starch
Nanoparticle
Hydrogel
Biopolymer
Photopolymerization
Sustainable materials

ABSTRACT

Starch is an attractive biomaterial given its low cost and high protein repellency, but its use in forming functional hydrogels is limited by its high viscosity and crystallinity. Herein, we demonstrate the use of fully amorphous starch nanoparticles (SNPs) as functional hydrogel building blocks that overcome these challenges. Methacrylation of SNPs enables hydrogel formation via photopolymerization, with the low viscosity of SNPs enabling facile preparation of pre-gel suspensions of up to 35 wt% SNPs relative to < 10 wt% with linear starch. Small angle neutron scattering indicates a significantly different microstructure in SNP-based hydrogels compared to linear starch-based hydrogels due to the balance between inter- and intra-particle crosslinks, consistent with SNPs forming denser and stiffer hydrogels. Functionalized SNPs are highly cytocompatible at degree of substitution values < 0.25 and, once gelled, can effectively repel cell adhesion. The physicochemical versatility and biological functionality of SNP-based hydrogels offer potential in various applications.

1. Introduction

The use of starch as a hydrogel building block has attracted growing interest due to its low cost, renewability, and ready availability (Elvira, Mano, San Román, & Reis, 2002; Ismail, Irani, & Ahmad, 2013). For biomedical applications, the innate enzymatic degradability of starch into glucose (Malafaya, Silva, & Reis, 2007; Van Vlierberghe, Dubruel, & Schacht, 2011) coupled with its highly hygroscopic nature (Ramaraj & Radhakrishnan, 1994) offer advantages for enabling clearance while maintaining high water contents and thus minimal protein adsorption/cell adhesion. While multiple starch-based hydrogels have been reported (Ismail et al., 2013), the high viscosity, high degree of crystallinity that can impede water binding and reduce the reactivity of hydroxyl groups for functionalization (Norisuye et al., 2002), and large batch-to-batch and source-to-source variability of starch (Wang, Hasjim, Wu, Henry, & Gilbert, 2014) all pose challenges to its practical use for hydrogel fabrication.

As an alternative to using linear starch as a hydrogel building block, starch nanoparticles (SNPs) offer multiple beneficial properties. In general, nanoparticles may be covalently or physically associated with another hydrogel, physically encapsulated another bulk hydrogel matrix, or (if they are themselves gels) comprise the hydrogel matrix without any additional materials (Thoniyot, Tan, Karim, Young, & Loh, 2015). The incorporation of nanoparticles into hydrogels has been demonstrated to (1) increase the density and, by extension, alter the mechanics of the gel network, (2) control the diffusion and/or partitioning and thus release of a payload; (3) introduce differential degradability into the hydrogel; and/or (4) produce useful optical properties (Dannert, Stokke, & Dias, 2019; Sivakumaran, Maitland, & Hoare, 2011). Both starch nanoparticles (Qiu et al., 2016; Zhang et al., 2013)

Abbreviations: SNP, starch nanoparticle; SS, soluble starch; MAAn, methacrylic anhydride; DS, degree of substitution; AGU, anhydrous glucose unit; UV, ultra-violet; ^{1}H-NMR, proton nuclear magnetic resonance; NTA, nanoparticle tracking analysis; DLS, dynamic light scattering; GPC, gel permeation chromatography; TEM, transmission electron spectroscopy; SANS, small angle neutron scattering; FITC, fluorescein isothiocyanate; pMMA, poly(methyl methacrylate); pNIPAM, poly(N-isopropylacrylamide; PVAm, poly(vinylamine); IPN, interpenetrating network; KPS, potassium persulfate; TDA, triazolinedione; BAC, N,N'-bis(acryloyl) cystamine; BIS, *N,N*-methylenebis(acrylamide); SDS, sodium dodecyl sulfate; WCSNPs, waxy corn starch nanoparticles; PSNPs, potato starch nanoparticles; PVA, poly(vinyl amine); DMEM, Dulbecco's modified Eagle's medium; FBS, fetal bovine serum; PS, penicillin streptomycin; DMSO, dimethyl sulfoxide

* Corresponding author.
E-mail addresses: majcherm@mcmaster.ca (M.J. Majcher), carter.l.mcinnis@gmail.com (C.L. McInnis), himberts@mcmaster.ca (S. Himbert), alsoprj@mcmaster.ca (R.J. Alsop), dkinio@ecosynthetix.onmicrosoft.com (D. Kinio), markus.bleuel@nist.gov (M. Bleuel), rheinsm@mcmaster.ca (M.C. Rheinstädter), NSmeets@walkerind.com (N.M.B. Smeets), hoaretr@mcmaster.ca (T. Hoare).

https://doi.org/10.1016/j.carbpol.2020.115998
Received 27 November 2019; Received in revised form 8 February 2020; Accepted 11 February 2020
Available online 12 February 2020
0144-8617/

and starch nanocrystals (Bel Haaj, Thielemans, Magnin, & Boufi, 2016; Lin, Huang, & Dufresne, 2012) have been explored as potential nanoparticle fillers in this context to create nanocomposite hydrogels both via simple physical incorporation (Kheradvar, Nourmohammadi, Tabesh, & Bagheri, 2018) (S. Li, Xia, Qiu, Chen, & Shi, 2018) as well as chemical grafting (Sheeja et al., 2018) (Saragih, Tamrin, Marpongahtun, Nasution, & Abdillah, 2018); in a few cases, multifunctional SNPs have been used as crosslinkers to form hydrogels (Y. Li et al., 2014) or networks with other nanoparticles (Lima-Tenório et al., 2015). Significantly fewer reports of all-nanoparticle hydrogels in which nanoparticles are directly crosslinked together to form the hydrogel network have been published, with network formation having been achieved via double layer repulsion of dense nanoparticle suspensions (Jia, Tang, Guan, & Zhang, 2018; Maurer, Condon, McKinney, & Kim, 2009), photopolymerization (Thaiboonrod, Milani, & Saunders, 2014), click chemistry (Absil et al., 2016), and temperature-induced gelation (Gaulding, Smith, Hyatt, Fernandez-Nieves, & Lyon, 2012). However, aside from the chiral nematic self-gelation of cellulose nanocrystals that forms gels that are inherently unstable to dilution (Abitbol & Cranston, 2014), to our knowledge no sustainable nanoparticle network hydrogel composed of solely nanoscale building blocks has yet been reported.

Effective formation of an SNP-based hydrogel is dependent on the formation of amorphous and reproducible SNPs. Traditional methods for fabricating SNPs include the precipitation of amorphous starch granules (Ma, Jian, Chang, & Yu, 2008; Tan et al., 2009), complex formation and enzymatic hydrolysis (Kim & Lim, 2009), microfluidization-based homogenization (Liu, Wu, Chen, & Chang, 2009), and ultrasound treatment (Bel Haaj, Magnin, Pétrier, & Boufi, 2013; H. Y. Kim, Han, Kweon, Park, & Lim, 2013; Zhu, Li, Chen, & Li, 2012). However, all these methods result in highly variable particle size distributions and morphologies. Newer strategies offer other challenges; for example the surfactant-regulated self-assembly of size-controlled SNPs upon enzymatic hydrolysis (X. Li et al., 2016) results in narrowly dispersed 15 – 35 nm SNPs but offers limited scalability (Sun, Li, Dai, Ji, & Xiong, 2014) while chemical extraction of phytoglycogen nanoparticles naturally existing in certain corn varieties creates highly monodisperse nanoparticles but is resource-intensive and results in dendritic rather than gel-like nanoparticles (Grossutti, Bergmann, Baylis, & Dutcher, 2017; Nickels et al., 2016). A more scalable strategy involves a process in which starch is gelatinized, “regenerated” via a secondary process, and then further cross-linked to form a nanoparticle (Deborah Le Corre & Angellier-Coussy, 2014; Sun et al., 2014). Reactive co-extrusion is one such process, by which native starch granules (~ 30 μm) are plasticized and subsequently crosslinked within a twin screw extruder to yield fully amorphous 20 – 50 nm SNPs (Bloembergen et al., 2010; Ip, Tsai, Khimji, Huang, & Liu, 2014; Tseitlin et al., 2012). The extremely high specific surface area of these SNPs, coupled with the potential for high-density surface functionalization of the fully amorphous nanoparticles, makes such SNPs attractive building blocks for hydrogels. Specifically, we hypothesize that using reactive co-extrusion processed and functionalized starch nanoparticles as building blocks for hydrogel formation will facilitate the formation of denser and stiffer hydrogels than can be achieved with linear starch. In particular, the potential to leverage both intra-particle and inter-particle crosslinking to regulate hydrogel properties, coupled with the ease of functionalization of the fully amorphous SNPs, will enable the design of highly tunable biopolymer hydrogels for biomedical applications.

Herein, we apply SNPs fabricated via reactive extrusion and subsequently methacrylated via a highly scalable chemistry to fabricate SNP-based nanoparticle network hydrogels via photopolymerization. SNP-based hydrogels can be prepared at ~4-fold higher mass concentrations relative to linear starch-based hydrogels while also exhibiting enhanced mechanics, low cytotoxicity, and high cell repulsion. In addition, the internally crosslinked structure of the 20 – 50 nm SNP building blocks is shown to substantially alter the internal morphology of the resulting hydrogel without negatively impacting (or, in some cases, improving) the biological properties of the hydrogels.

2. Materials & methods

2.1. Materials

Experimental grade starch nanoparticles (SNPs) and experimental grade cold water-soluble linear starch (SS) (both waxy starches with 100 % amylopectin and a fully amorphous internal structure, **Supplementary Figure S1**) were provided by EcoSynthetix Inc. (Burlington, ON). Methacrylic anhydride (MAAn, 94 %), Irgacure 2959 photoinitiator (98 %), bovine serum albumin (BSA) (≥ 98 %), fluorescein isothiocyanate isomer I (FITC) (≥ 97.5 %), and resazurin sodium salt (80 %) were all obtained from Sigma Aldrich (Oakville, ON) and used as received. 3T3 *Mus musculus* mouse fibroblast cells were obtained from ATCC Cedarlane Laboratories (Burlington, ON) and cultured in Dulbecco’s modified Eagle’s medium (DMEM) supplemented with 10 % fetal bovine serum (FBS) and 1% penicillin streptomycin (PS) (all from ThermoFisher). Trypsin-EDTA and calcein AM/ethidium homodimer live/dead assay kits were obtained from Invitrogen. For all experiments, Millipore Milli-Q grade distilled deionized water (MQW, 18.2 MΩ cm resistivity) was used.

2.2. Synthesis of methacrylated starch

SNPs were functionalized with methacrylate groups using a method adapted from literature (Bae et al., 2011). Briefly, a 25 w/v% dispersion of 50 g dry weight of SNPs and 0.7 g of sodium carbonate in MQW was created using an IKA homogenizer operating at 12,000 rpm. Subsequently, a pre-determined amount of MAAn to target degree of substitution (DS) values of 0.25 (11.44 mL MAAn), 0.10 (4.56 mL MAAn), 0.050 (2.29 mL MAAn), and 0.015 (0.69 mL) was added dropwise over a period of 60 min while the reaction temperature and pH were held at 25 °C and 10.4 respectively, the latter through the addition of 1 M sodium hydroxide (NaOH) as required. The reaction was run for an additional 30 min, after which the pH was neutralized to pH 7 using 1 M hydrochloric acid (HCl) and the product was dialyzed against MQW over 6 × 6 h dialysis cycles using a 3.5 – 5 kDa molecular weight cut-off membrane. The same procedure was followed to methacrylate the cold water-soluble linear starch control (SS) at the same DS values, but the w/v% of the SS was lowered to 7.5 w/v% to compensate for the higher viscosity and molecular weight of SS versus SNPs. **Supplementary information Figure S2** shows a detailed mechanism of the esterification reaction performed using MAAn.

2.3. Chemical characterization of functionalized starch

The degree of substitution (DS) of methacrylate groups on both modified SNP and SS samples was analyzed using ^{1}H nuclear magnetic resonance (Bruker AVANCE 600 Hz ^{1}H-NMR) by comparing the intensities of the vinylic protons (δ = 5.8 and 6.2 ppm) with that of the anomeric α-carbon present on each functional unit of the glucose backbone (δ = 5.4 ppm); see the representative ^{1}H-NMR spectra in **Supplementary information Figure S3 (a, b)** and data summary in **Supplementary information Table S1**. A comparison between the theoretical/targeted DS and the experimental/actual DS is also provided in **Supplementary information Figure S4**.

2.4. Physical characterization of starch hydrogel precursors

The hydrodynamic radius, refractive index, and molecular weight distribution of unmodified and methacrylated SNPs and SS were analyzed using a Viscotek GPCmax and Triple Detection Array 305 (Malvern) using an Aquagel PAA-200 series column (PolyAnalytik). All samples were run at room temperature at 3 – 5 w/v% using dimethyl

sulfoxide (DMSO) containing 0.05 M lithium bromide as the solvent and pullulan as the calibration standard. The particle size of SNPs before and after functionalization was analyzed using three methods: (1) Dynamic light scattering (DLS) was run at a particle concentration of 0.1 wt% (count rate 150–200 kcps) in a 1 mM sodium chloride solution following water bath sonication for 5 – 10 min at room temperature prior to analysis to reduce aggregation. The reported average particle sizes/error bars represent the averages/standard deviations of four independent measurements (**Supplementary information Figure S5(a, b) and Table S2**); (2) Nanoparticle tracking analysis (NTA, NanoSight LM10) was used to measure the number particle size distribution. All samples were run at a concentration of 100 μg/mL in MQW and sonicated for 5 – 10 min prior to testing as described for DLS measurements to ensure good SNP dispersibility (**Supplementary information Figure S6**); (3) Transmission electron microscopy (TEM) was performed using a JEOL 1200EX TEMSCAM instrument to assess particle size and structure. In order to prevent film formation of SNPs on the TEM grid, a low contrast poly(methyl methacrylate) (PMMA) latex (particle size = 300 nm) was used as an imaging aid by aliquoting 0.5 wt% SNPs with 0.1 wt% PMMA latex dispersions on a standard carbon/Formvar TEM grid and drying overnight prior to measurement. Average particle size results are reported based on the average of the sizes reported from ImageJ analysis of 30–40 particles, with the error bar representing the standard deviation.

2.5. Formation of SNP and SS hydrogels

To fabricate all-SNP nanoparticle network hydrogels, 35, 25, or 10 wt% dispersions of methacrylated SNPs were prepared in MQW following homogenization using an IKA overhead homogenizer operating at 10,000–12,000 rpm; the solids content of each "dry" SNP sample was confirmed using a CEM microwave dryer to ensure consistency in dry SNP contents between the prepared hydrogels. Subsequently, for every 1 mL of starch solution, 100 μL of a 1.5 w/w% Irgacure 2959 solution in DMSO was added to the pre-gel dispersion, yielding a final concentration of 0.15 wt% of Irgacure 2959. Following 5 – 10 min of vortexing, the samples were pipetted into a 12.7 mm diameter/4 mm thick silicone mold and then irradiated at a wavelength of 365 nm using a CureAll lamp (80 mW/cm^2 power) for 10 min., an irradiation time chosen based on a preliminary gelation kinetics experiments (see **Supplementary information, Table S3**). Fig. 1 summarizes the full fabrication scheme used to generate the SNP hydrogels. Hydrogels based on SS precursors were prepared using the same protocol but using lower starch concentrations (10, 7.5 and 5 wt% SS) accounting for the high viscosity of the SS precursor polymers.

2.6. Hydrogel characterization

Gravimetry was used to track both hydrogel swelling and degradation over time. Samples were prepared as described in section 2.5 and subsequently incubated in 10 mL of 10 mM PBS at 37 °C using cell culture inserts (0.4 μm pore size) inserted in 12-well plates. The equilibrium swelling ratio was defined as the point at which the rate of gel mass change between two consecutive samples was statistically insignificant via a two-tailed *t*-test ($\alpha = 0.05$). The mechanical properties of the hydrogels were assayed using the same hydrogel disks using a MACH-1 micromechanical tester (Biomomentum Inc., Laval, Canada). A strain sweep was performed spanning an amplitude of 0.1 deg to 2.154 deg at a frequency of 1 Hz to identify the linear viscoelastic range; following, a frequency sweep was performed using 1% strain over a frequency range of 0.1 Hz–2.154 Hz to determine the storage (*G'*) and loss (*G"*) moduli. The raw data was analyzed using the sinusoidal analysis function on the MACH-1 analysis software.

2.7. Gel microstructure

Both dispersions and gels of SNPs were analyzed using the NGB 30 m small angle neutron scattering (SANS) instrument at the NIST Center for Neutron Research (NCNR) in Gaithersburg, MD, USA. Gel samples were fabricated inside the NCNR's standard titanium sample holders equipped with two quartz windows (19 mm diameter, 2 mm path length) by photopolymerizing gels of the same compositions described above. For SNP dispersions, the "fuzzy sphere" model of Stieger et al. (Stieger, Pedersen, Lindner, & Richtering, 2004) with an additional square well potential to account for aggregation (Sharma & Sharma, 1977) (**Equations 1 & 2**) was used to fit the SANS data, allowing for extraction of the radius of the SNPs (R), the polydispersity of the SNPs, the width of "fuzzy" interface σ (although fitting was effective in each case when this value was manually set to 0 for all samples, suggesting that SNPs can be modeled as homogeneous spheres rather than fuzzy spheres), and the Ornstein-Zernike Lorentzian correlation length ξ (related to the mesh size of the internal gel network).

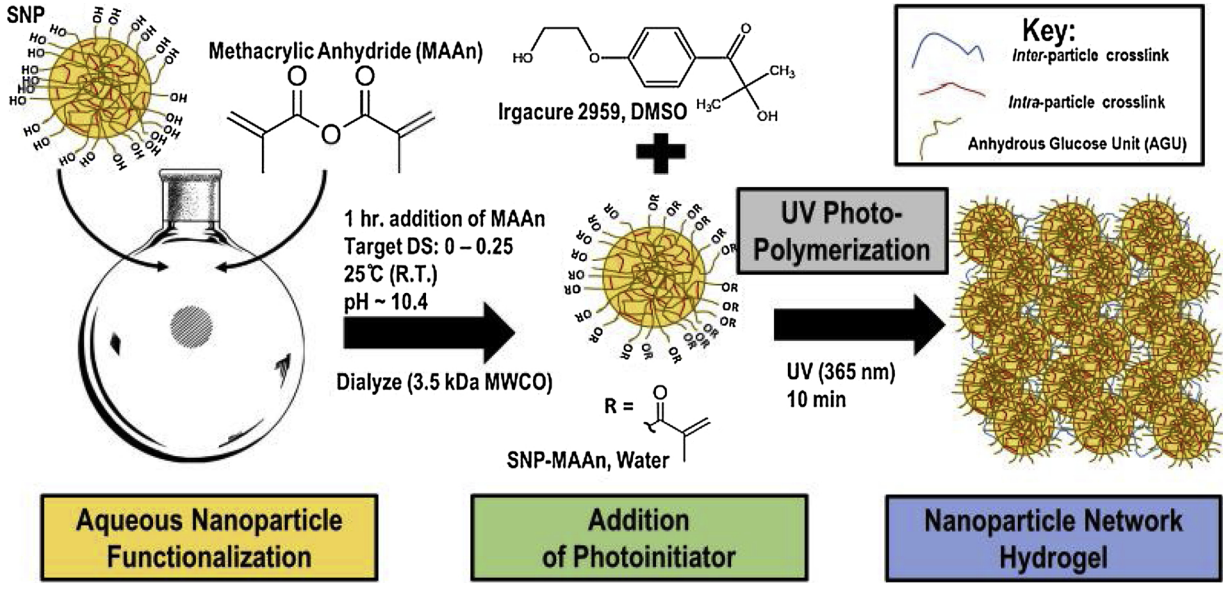

Fig. 1. Experimental protocol for methacrylation and subsequent photogelation of SNP-based nanoparticle network hydrogels.

$$I(q) = \frac{scale}{V}(\Delta\rho)^2\langle A^2(q)\rangle S(q) + \frac{I_{lor}(0)}{1+\xi^2 q^2} + bkg \quad (1)$$

$$A(q) = \frac{3[\sin(qR) - qR\cos(qr)]}{(qR)^3} exp\left(\frac{-(\sigma_{surf}q)^2}{2}\right) \quad (2)$$

Note that the structure factor *S(q)* was set equal to 1 for all *q* in the case of diluted solutions.

SNP hydrogel data were fitted to the Porod model (Eq. (3)) that describes networks in the absence of static inhomogeneities (Gilbert et al., 2017; Hammouda, Ho, & Kline, 2004):

$$I(Q) = \frac{s_{porod}}{Q^n} + \frac{s_{oz}}{1+(Q\xi)^m} + bkg \quad (3)$$

Here, s_{porod} and s_{oz} measure the scale of the Porod and Ornstein Zernike functions, n is the low-q Porod exponent describing clustering and swelling within a network (Hammouda, 2004), ξ is the correlation length of the network indicative of gel mesh size, m is the Lorentzian exponent quantifying polymer-solvent interactions, and *bkg* is the incoherent background. All fits were performed using Igor Pro (Software Version 6.37) together with the SANS reduction and analysis macro provided by the NCNR.

2.8. In vitro cytotoxicity assay and leachate test

The cytocompatibility of the SNP and SS precursor solutions used was assessed using a resazurin assay. NIH 3T3 *Mus musculus* fibroblasts were plated at a density of 10,000 cells per well in a 96-well plate and maintained in DMEM media supplemented with 10 % FBS and 1% penicillin/streptomycin. Cells were cultured for 24 h at 37 °C and 5% CO_2 in 1 mL of DMEM, after which SNP or SS samples (both unmodified and methacrylated) at concentrations ranging from 0.1 − 10 mg/mL were added and cells were incubated for an additional 24 h. A resazurin solution was added to each well give a final concentration of 10 μg/mL resazurin and incubated for 8 h, after which the entire supernatant was removed, loaded into a 96 well plate, and analyzed on a plate reader (Infinite M200 Pro, Tecan; λ_{ex} = 560 nm, λ_{em} = 590 nm). All results were normalized using media and hydrogel-only blanks. Error bars represent the standard deviation of the measured cell viability percentages (n = 4 wells/sample).

To assess the potential cytotoxicity of any gel leachates, pre-formed hydrogel disks (6.35 mm diameter, 4 mm thickness) were incubated in 5 mL DMEM with 10 % FBS and 1% Pen-Strep for 1, 3, 5, and 7 days at 37 °C under 500 rpm shaking. Following, the samples were filtered using a 0.45 μm filter (Acrodisc) and frozen for storage (-20 °C). When all leachate samples were collected, the samples were thawed and 50 μL was added into a 96 well plate containing 10,000 NIH 3T3 cells/well (n = 6). Cytotoxicity was measured using the resazurin assay previously described.

2.9. In vitro cell adhesion assay

To assess the adhesion of cells to the hydrogels, 270 μL of each filtered polymer precursor solution was aliquoted into a 48-well plate. The precursors were photopolymerized at 365 nm for 10 min and left to sit for 1 h, after which they were swollen to equilibrium over 48 h following the addition of 600 μL of sterile 10 mM PBS to each well. The gels were washed with DMEM media, after which 10,000 NIH 3T3 cells in 600 μL media were plated in each well. The samples were incubated at 37 °C and 5 % CO_2 for 1, 3, 5, or 7 days, after which a LIVE/DEAD assay (2 mM calcein and 4 mM ethidium homodimer) was used to stain the cells. The samples were washed three times with sterile PBS to remove any weakly bound cells, after which the residual cells were imaged using excitation wavelengths of 525 nm (live) or 470 nm (dead) using an Olympus inverted microscope.

3. Results and discussion

3.1. Characterization of methacrylated SS and SNPs

Esterification of both soluble starch (SS) and SNPs with methacrylic anhydride introduces photopolymerizable methacrylate groups on starch. Degree of substitution (DS) values measured via ^{1}H NMR (**Supplementary information Table S1**) were lower than those predicted by stoichiometry but scaled with the predicted DS values (**Supplementary information Figure S4**), with the linear starch yielding a slightly higher DS than SNPs for most DS values tested. These results are consistent with the increasing steric barriers to methacrylation of a crosslinked starch nanoparticle relative to fully solubilized starch. The methacrylation reaction does not significantly affect the hydrodynamic diameter of either SS or SNPs in solution, with GPC analysis showing similar retention profiles for both SS and SNPs before and after methacrylation (Fig. 2(a, b)). Dynamic light scattering (DLS) analysis on SNPs confirms the independence of particle size on the DS value (**Table S2** and Table 1). Intensity-averaged DLS measurements (**Supplementary information Fig. S5)** indicate that SNPs have two sub-populations suggestive of minor aggregation in the sample independent of sample concentration: one centered at ~20 nm (20–40 % of scattered intensity) the other centered at 170 − 190 nm (90–100 % of scattered intensity). This result and interpretation are consistent with the NTA analysis (Fig. 2c and Table 1), which consistently reported sizes of ~180 nm for each SNP tested (note that the sizes of free SNPs are at or below the 30 nm lower limit of detection of NTA). Converting the intensity-weighted DLS results to number-weighted results by assuming a refractive index of 1.34 (between that of starch (1.40–1.44) and the water swelling the particles (1.30–1.33)), a single peak of freely non-aggregated SNPs appears with a size of ~20 nm independent of the DS of the SNP (Table 1**)**. This smaller base particle size is also consistent with the TEM results (average sizes in Fig. 2d from images in Fig. 2(e,f)), which show single SNP particles oriented along the outside edge of the PMMA latex particles (size 300 ± 15 nm) added to prevent SNP film formation. Thus, independent of the methacrylation DS value, SNP samples consist of a dominant fraction of small (20 − 30 nm) nanoparticles with a smaller fraction of aggregate that appears to form dynamically in suspension.

3.2. Physical characterization of photopolymerized SS and SNP hydrogels

Photoinitiation of the methacrylate groups grafted to the SNPs induces a typical free radical chain growth polymerization in suspension to crosslink SNPs together, with SNPs acting as multivalent macromonomers to form a bulk hydrogel. Note that the small size coupled with the high degree of internal hydration of the SNPs facilitates gelation compared to the use of a similar process with a “hard” nanoparticle, although a degree of both intraparticle and interparticle crosslinking within each SNP is likely to occur as a result of the close proximity of C═C groups within the SNPs. SS, as a non-crosslinked linear polymer, has higher conformational mobility than SNPs and crosslinks through a more typical solution-based gelation mechanism. Despite these differences in crosslinking phenomena based on the type of starch used, photopolymerization of all methacrylated SS and SNP samples yielded hydrogels within 10 min of UV exposure.

Of particular note, the significantly lower viscosity of SNPs relative to SS allowed for achieving much higher SNP weight percentages (as high as 35 wt%) in the precursor polymer solutions than achievable with SS (< 10 wt%). The elastic storage modulus (*G'*) as a function of the initial polymer concentration and the degree of methacrylation is shown in Fig. 3 for hydrogels prepared using different SNP (Fig. 3a) or SS (Fig. 3b) precursors, while the loss modulus (G") is reported in Fig. 3c and Fig. 3d, respectively. In either case, *G'* increases with the precursor polymer concentration and/or the DS of methacrylate groups, consistent with gelation theory. At equivalent DS and mass

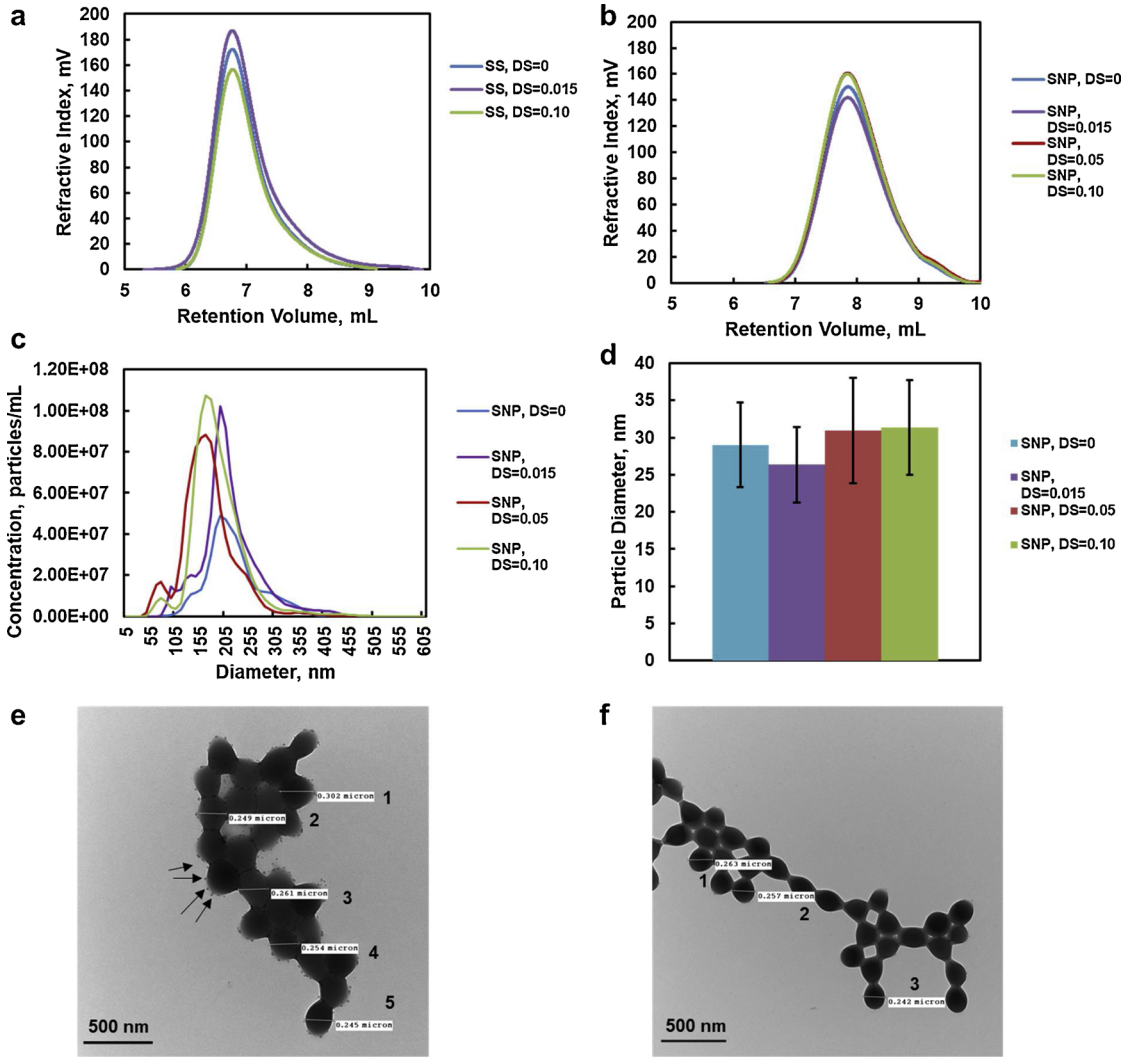

Fig. 2. (a-f): Particle sizes of SNPs and SS before and after methacrylation: (a, b) GPC traces for (a) SS and (b) SNP samples before and after methacrylation with different target DS values; (c) NTA results as a function of the degree of substitution of SNPs; (d) average particle sizes from TEM image analysis software for SNPs before and after methacrylation (30-40 individual particles were sized for each formulation); (e, f) TEM images of SNPs in a PMMA latex (e) relative to the PMMA latex alone (f) (scale bar = 500 nm). The numbers in (e) and (f) correspond to individual PMMA particles sized for comparison to the SNP average sizes reported in panel (d).

Table 1
Mean and mode diameters of SNPs before and after various degrees of methacrylation as measured by dynamic light scattering (0.1 wt% SNP concentration) and nanoparticle tracking analysis (100 μg/mL SNP concentration). See **Supplementary information Figure S5 and Table S3** for DLS sizing data at different dilutions.

Degree of Substitution	DLS Diameter (intensity-weighted) (nm)	DLS Diameter (number-weighted) (nm)	NTA Mean Diameter (nm)	NTA Mode Diameter (nm)
0	194 ± 8	21 ± 8	184 ± 41	178 ± 41
0.015	230 ± 30	14 ± 8	214 ± 68	202 ± 68
0.05	242 ± 8	21 ± 5	178 ± 48	161 ± 48
0.10	287 ± 14	17 ± 5	184 ± 58	171 ± 58
0.25	270 ± 9	19 ± 6	186 ± 55	161 ± 55

concentrations (10 wt% polymer and DS = 0.25, the maximum concentration at which SS was soluble in water and the minimum concentration/DS at which SNPs could form a hydrogel), the *G'* of the SS-based hydrogels (*G'* ~ 1000 Pa) exhibited a modulus value double than that observed with SNP-based hydrogels (*G'* ~ 500 Pa), consistent with the linear SS hydrogels having more conformational mobility relative to the internally crosslinked SNPs at the same mass fraction. However, the significantly higher concentrations achievable with SNP-based hydrogels enabled the formation of much stiffer hydrogels using SNPs as the building block, with *G'* values up to ~6500 Pa achieved for 35 wt% SNP (DS 0.10) hydrogels; this is ~6-fold higher than the highest modulus achievable with SS. Similar trends were observed at the equilibrium swollen state (**Supplementary information** Fig. *S7*), although the absolute storage modulus values were reduced due to the influx of water into the network. Thus, by using SNPs as a hydrogel building block, significantly denser and stronger hydrogels can be fabricated without introducing processability/solubility complications.

Fig. 4(a–f) show the equilibrium volumetric swelling ratios of SS and SNP-based hydrogels prepared at various DS values and mass concentrations (see **Supplementary information,** Fig. S**8** for the corresponding swelling kinetics data). For both SS and SNP-based hydrogels, increasing either the DS or the mass concentration of the precursor

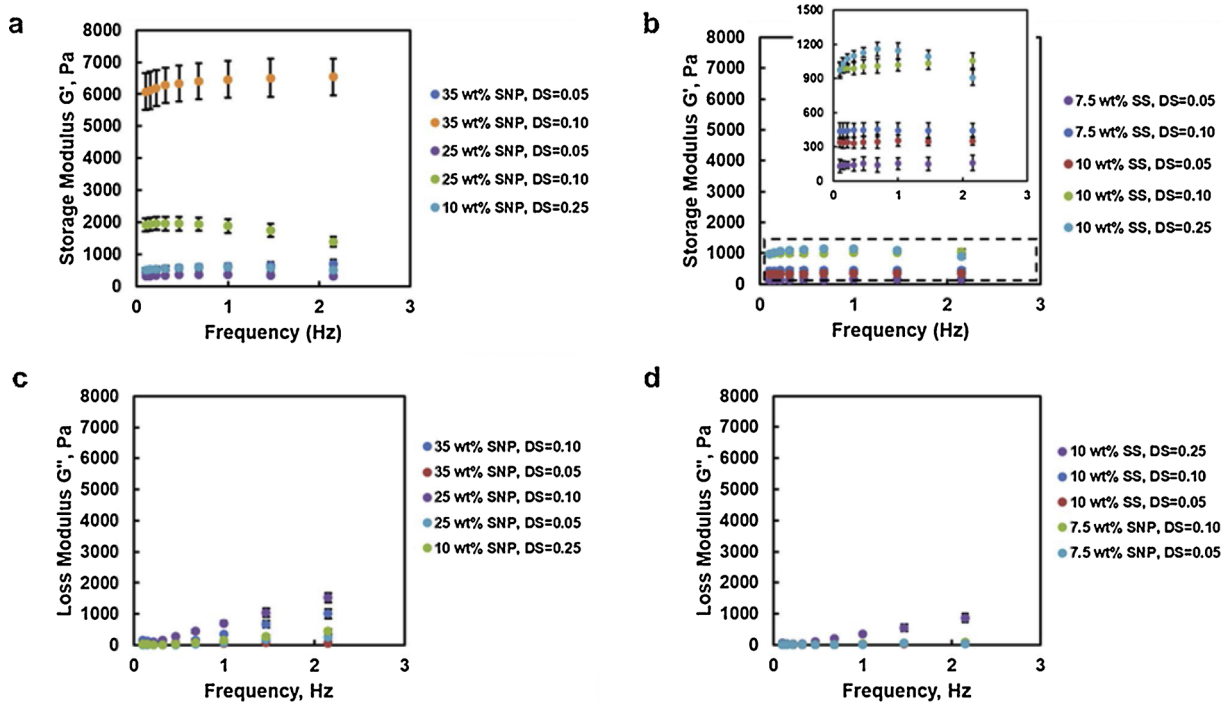

Fig. 3. (a, b) Shear storage modulus (*G'*) as a function of strain frequency for hydrogels prepared with (a) SNP building blocks and (b) SS building blocks at various concentrations and DS values (insert of (b) is a zoom-in between moduli of 0-1500 Pa to more clearly show differences between the weaker SS hydrogel mechanics with the same x and y axis information); (c,d) Shear loss modulus (*G"*) as a function of strain frequency for hydrogels prepared with (c) SNP building blocks and (d) SS or lower concentration SNP building blocks at various concentrations and DS values.

units results in a reduction of the equilibrium degree of swelling, consistent with the mechanical testing results (Fig. 3) and the typical link between increasing crosslink density and reducing swelling. However, clear differences were observed between the SS and SNP-based hydrogel series. At an equivalent 0.25 DS/10 wt% mass concentration, the equilibrium swelling degree of SNP-based hydrogels was slightly higher than that achieved with SS-based hydrogels, consistent with the weaker mechanics of the SNP-based hydrogel at this DS/concentration value due to the internal SNP crosslinks restricting inter-particle crosslinking (Fig. 3a). However, the higher mass concentrations achievable with SNP hydrogels allow for significant reductions in the equilibrium degrees of swelling that are achievable, with the highest concentration/DS SNP-based hydrogel that could be fabricated swelling less than half that of the highest concentration/DS SS-based hydrogel that could be fabricated (Fig. 4). This result is attributable to both the higher wt% of the SNP hydrogels (introducing more photopolymerizable crosslinking points in the same hydrogel volume at equivalent DS values) and the pre-existing internal crosslinks within the SNPs themselves that act as an additional elastic driving force for limiting swelling. On this basis, using SNPs can maintain the beneficial properties of starch as a hydrogel building block but achieve both stiffer and lower swelling hydrogels than possible with conventional starch.

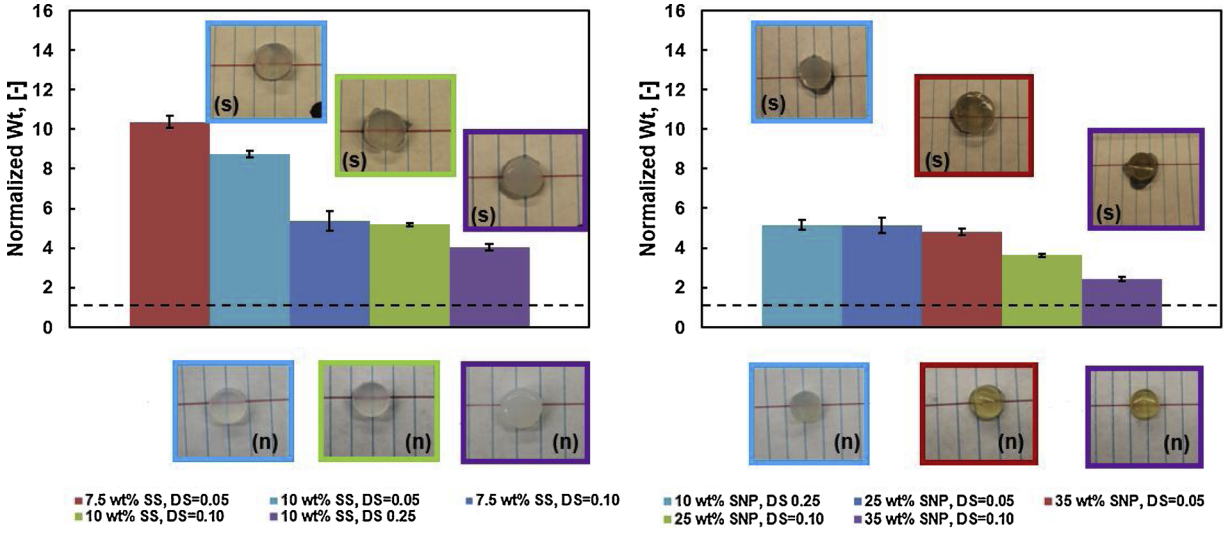

Fig. 4. Equilibrium swelling ratios (relative to the dry state) for hydrogels prepared with SNP building blocks (a, left) and hydrogels prepared with SS building blocks (b, right). Photographs of selected hydrogel formulations are included below in the neat state (n) and above in the equilibrium swollen state (s), with the color of the border around each photograph corresponding to the colors in the legend in each respective figure. Note that the dotted line represents the starting weight (pre-swelling) normalized to a value of 1.

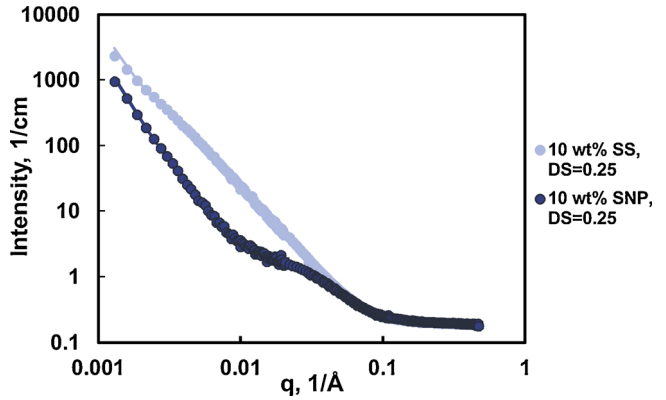

Fig. 5. Representative SANS curves for 10 wt%/DS 0.25 hydrogels based on (a) SNPs (lighter blue) and (b) SS (darker blue) (For interpretation of the references to colour in this figure legend, the reader is referred to the web version of this article).

3.3. Small angle neutron scattering

Small angle neutron scattering (SANS) was performed to compare the internal morphology of the SNPs before and after methacrylation. **Supplementary information Table S4** shows the key fitting results for single SNPs before and after methacrylation; for raw SANS data and best-fit lines, see **Supplementary information Fig. S9**. The SNP diameter was determined to be ~160−170 nm independent of DS, fully consistent with the results obtained from DLS and NTA (Table 1). In addition, neither the particle scattering length density (related to the water content of the SNP) nor the correlation length (related to the internal distance between inhomogeneities/crosslinks in the sample) significantly change before and after methacrylation. This analysis further confirms that methacrylation has no significant impact on the SNP structure, allowing us to relate all observed property changes to changes in the SNP interparticle crosslink density imparted by the different degrees of methacrylation/starch concentrations.

Fig. 5 shows representative SANS curves and fits for an SNP-based hydrogel relative to a SS-based hydrogel, while Table 2 shows a summary of the key SANS parameters for the SNP nanoparticle networks; all collected SANS graphs are available in **Supplementary information Figures S10-S15** and the full set of corresponding best-fit parameters are presented in **Table S5**.

Qualitatively (Fig. 5), SS and SNP-based hydrogels show similar curve shapes in the high q region (consistent with similarities in the starch polymer chain structures) but significant deviations in curve shapes at the low q region indicative of the different length scales of crosslinking between individual chains/particles in each sample. Based on the best-fit parameters (Table 2), SS hydrogels correspondingly have significantly lower Porod exponents (corresponding to more Gaussian, swollen chains), significantly higher Lorentzian screening lengths (indicating larger gel mesh sizes), and much larger Lorentzian scales (indicating a significantly more fluid network structure) than SNP-based hydrogels. All these observations are consistent with replacing a soluble linear starch with a smaller but internally crosslinked SNP as the hydrogel building block. Within the SNP-only hydrogels, increasing the wt% of SNPs used to prepare the hydrogel results in a relatively unchanged Porod exponent (suggesting minimal changes to the fractal nature and thus internal swelling of the SNP building blocks themselves) but a marked decrease in both the Lorentzian screening length (i.e. internal mesh size) and Lorentzian scale (i.e. the relative contribution of the fluid-like inhomogeneities to the overall scattering observed), both consistent with the creation of denser and more crosslinked hydrogel networks. Similarly, as the DS is increased at a single wt% of SNPs (25 wt%), the Porod exponent again remains relatively unchanged while decreases are again observed in both the Lorentzian screening length and the Lorentzian scale, consistent with the production of more crosslinked SNP-based hydrogels as a result of the higher degree of SNP methacrylation. Thus, the SANS results suggest that the degree of *inter-particle* crosslinking is substantially changed when either the SNP concentration or degree of methacrylation are changed (as evidenced by the trends in each of the Lorentzian/fluid-like fluctuation terms) but the *internal* structure/swelling of the SNP does not appreciably change (as evidenced by the relatively constant Porod exponent). Note that the constant Porod exponent also suggests that the small SNP aggregate fraction consistently observed in suspension (Fig. 2) does not introduce significant heterogeneities in the photo-crosslinked hydrogels.

3.4. In vitro cell studies

To assess the cytotoxicity of SNPs alone as well as the effect of methacrylation on the cytotoxicity of SS and SNPs, a resazurin assay was performed using 3T3 mouse fibroblasts (Fig. 6). Neither SS nor SNPs exhibited significant cytotoxicity at any concentration tested prior to methacrylation. High cytocompatibility (> 80 % relative to the cell-only control) was also maintained for DS = 0.05 modified SS and SNPs as well as DS = 0.10 modified SS across the full range of concentrations tested. However, moderate toxicity was noted for DS = 0.10 SNPs at the highest concentration tested (10 mg/mL) while significant cytotoxicity was observed for DS = 0.25 SS and SNPs at concentrations of 0.5 mg/mL and above. This observation is most likely related to the reactivity of free methacrylates to cells via Michael addition reactions with cell-bound proteins (Jackson, Widen, Harki, & Brummond, 2017) and/or to cellular glutathione (Ansteinsson, Kopperud, Morisbak, & Samuelsen, 2013). While the rapid photogelation achieved will consume most of these free methacrylate groups, these results suggest limiting the DS to 0.10 or less in any practical biomedical application.

To assess cell interactions with SNP and SS-based hydrogels, we performed two assays: (1) a qualitative assessment of cell adhesion to the hydrogels based on LIVE/DEAD staining of residual adhered cells following washing (Fig. 7) and (2) a leachate study to assess the potential cytotoxicity of the hydrogels to cells over time (Fig. 8). Together, these studies permit a full assessment of the anti-fouling properties of

Table 2
Key SANS parameters for photopolymerized hydrogels prepared with soluble starch (SS) compared with starch nanoparticles (SNPs).

Parameter	10 wt% SS, DS = 0.10	10 wt% SNP, DS = 0.10	25 wt% SNP, DS = 0.10	25 wt% SNP, DS = 0.05	25 wt% SNP, DS = 0.015	35 wt% SNP, DS = 0.10
Porod Exponent	2.74 ± 0.01	2.54 ± 0.05	2.42 ± 0.04	2.38 ± 0.03	2.82 ± 0.01	2.68 ± 0.09
Lorentzian Exponent	2.55 ± 0.01	2.51 ± 0.01	2.69 ± 0.02	2.77 ± 0.03	3.27 ± 0.04	2.71 ± 0.02
Lorentzian Screening Length (nm)	18.8 ± 0.5	13.1 ± 0.2	9.2 ± 0.2	8.8 ± 0.2	2.41 ± 0.02	16.4 ± 3
Lorentzian Scale	166 ± 3	65 ± 3	14.3 ± 0.7	11.8 ± 0.7	0.43 ± 0.01	87 ± 5

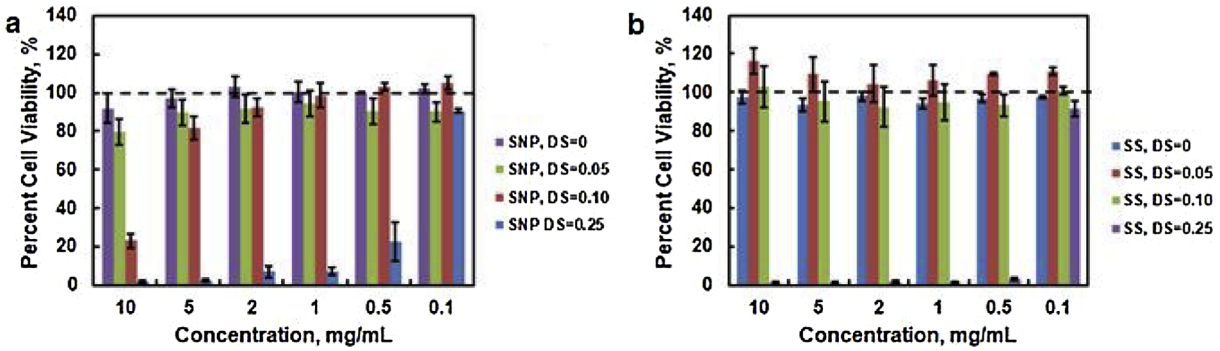

Fig. 6. In vitro cell viability of 3T3 mouse fibroblasts based on the resazurin assay for (a) SNPs and (b) SS over a range of DS values.

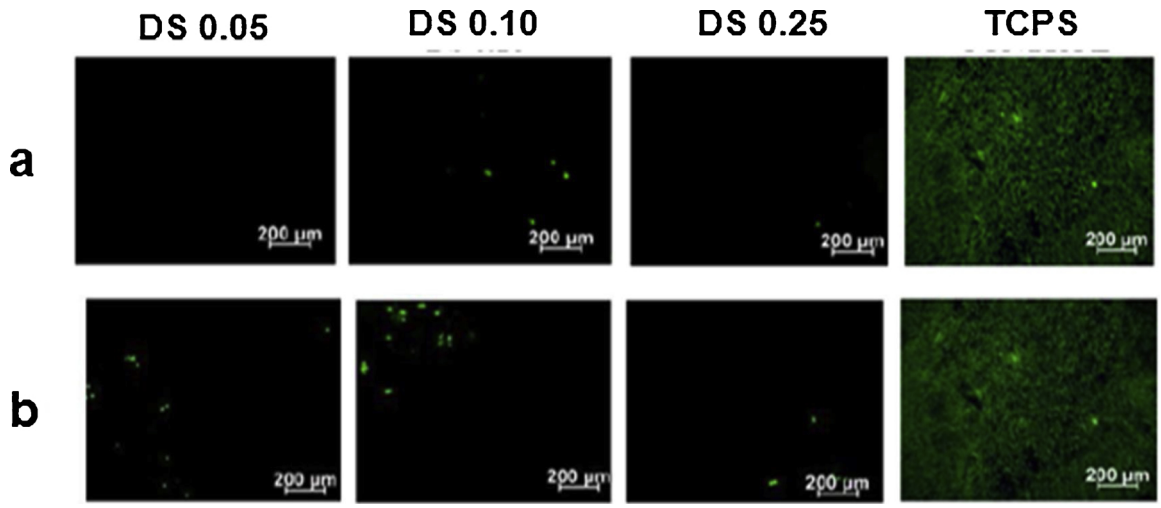

Fig. 7. 3T3 mouse fibroblast adhesion to hydrogels prepared from (a) SNP and (b) SS building blocks with different degrees of substitution (DS) relative to a tissue culture polystyrene control after 5 days of incubation (LIVE/DEAD staining).

the hydrogels wh ile controlling for potential complications due to cell death rather than inherent anti-fouling properties. Both SS and SNP hydrogels showed minimal adhered and viable cells at all DS values following three washes in 10 mM PBS after five days of cell incubation, a time over which the cells become confluent on the tissue culture polystyrene (TCPS) controls (Fig. 7). Correspondingly, the leachates from the gels exhibited no significant cytotoxicity (Fig. 8) aside from the DS 0.25 samples already noted as being cytotoxic (Fig. 6). Combined, these results suggest that the lack of cell adhesion is an inherent property of the DS 0.05 and DS 0.10 samples. Slightly more cells adhered to the SNP samples (attributable to the lower water concentrations in these materials, Fig. 4) and to DS 0.10 samples (higher crosslink density/stiffer substrate but still no cytotoxic leachates); however, overall, all the SS and SNP materials tested are non-adherent to even strongly adherent fibroblast cells. Note that the toxicity observed at higher DS values further emphasizes the benefits of using SNP building blocks that allow for accessing stiffer gels at lower degrees of methacrylation (Fig. 3) that will not induce any cytotoxicity.

4. Conclusions

Starch nanoparticles fabricated via reactive co-extrusion are demonstrated to be a relevant and useful starting material for the design of hydrogel systems based on their neutral surface charge, their surface rich in hydroxyl groups for subsequent modification (here, methacrylation to enable photopolymerization), their small size (< 50 nm), their

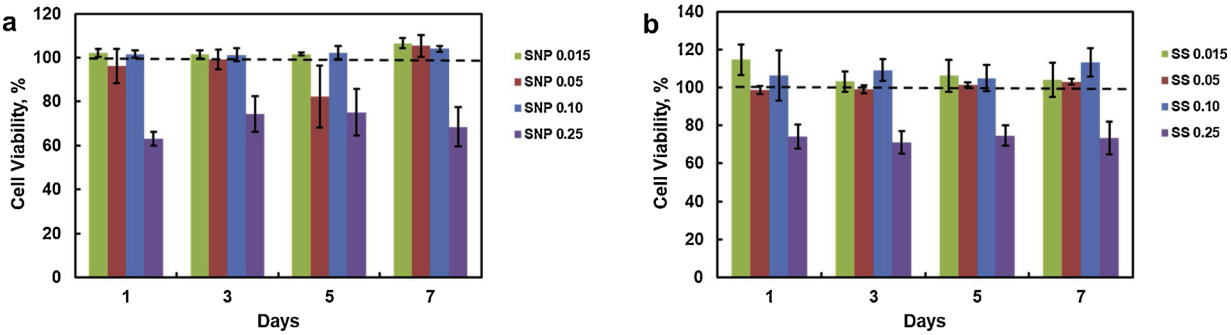

Fig. 8. Cell viability (via the resazurin assay) of 3T3 fibroblasts after 24 h of incubation with leachate samples from hydrogels made of (a) SS or (b) SNP building blocks soaked in DMEM media for different periods of time.

low cost, and their generally safe degradation products (glucose). Relative to linear starch hydrogels prepared at the same degree of methacrylation, hydrogels fabricated from SNP precursors can achieve at least five-fold higher shear moduli while demonstrating at least two-fold lower swelling ratios. This result was attributed to the dual intraparticle/interparticle crosslinking structure of the SNP-based hydrogels, as confirmed and elucidated via small angle neutron scattering analysis. Furthermore, provided the DS is limited to 0.10 or lower, SNP-based hydrogels exhibited high cytocompatibility and very low cell adhesion over a 7 day period, with SNP building blocks enabling access to stiffer gels that are inaccessible using soluble starch building blocks without inducing cytotoxicity. On this basis, SNP-based hydrogels are attractive options for fabricating stiffer but still highly cytocompatible and anti-biofouling hydrogels based on natural and degradable polymer precursors.

Funding sources

The Natural Sciences and Engineering Research Council of Canada (NSERC, Strategic Project Grant 463327-14) is gratefully acknowledged for funding this work. This work utilized facilities supported in part by the National Science Foundation under Agreement No. DMR-0944772. We acknowledge the support of the National Institute of Standards and Technology, US Department of Commerce, in providing the neutron facilities used in this work. Use of facilities provided by McMaster's Biointerfaces Institute and EcoSynthetix Inc. is also gratefully acknowledged.

Disclaimer

Certain commercial equipment, instruments, or materials are identified in this paper to foster understanding. Such identification does not imply recommendation or endorsement by the National Institute of Standards and Technology, nor does it imply that the materials or equipment identified are necessarily the best available for the purpose.

CRediT authorship contribution statement

Michael J. Majcher: Conceptualization, Methodology, Validation, Formal analysis, Investigation, Data curation, Writing - original draft, Writing - review & editing, Visualization. **Carter L. McInnis:** Methodology, Validation, Formal analysis, Investigation. **Sebastian Himbert:** Formal analysis, Software, Writing - review & editing. **Richard J. Alsop:** Investigation, Formal analysis, Software. **Dennis Kinio:** Methodology, Validation. **Markus Bleuel:** Resources, Software. **Maikel C. Rheinstädter:** Supervision. **Niels M.B. Smeets:** Supervision, Resources, Conceptualization, Funding acquisition. **Todd Hoare:** Supervision, Resources, Visualization, Writing - review & editing, Conceptualization, Funding acquisition.

Declaration of Competing Interest

The authors declare no competing financial interest.

Acknowledgments

The authors would also like to acknowledge Marcia Reid for her help with TEM and Dr. Boualem Hammouda for his help with acquiring the 30 m SANS data.

Appendix A. Supplementary data

Supplementary material related to this article can be found, in the online version, at doi:https://doi.org/10.1016/j.carbpol.2020.115998.

References

Abitbol, T., & Cranston, E. D. (2014). *Chiral nematic self-assembly of cellulose nanocrystals in suspensions and solid films. Handbook of green materials*37–56. https://doi.org/10.1142/9789814566469_0035.

Absil, R., Çakir, S., Gabriele, S., Dubois, P., Barner-Kowollik, C., Du Prez, F., ... Mespouille, L. (2016). Click reactive microgels as a strategy towards chemically injectable hydrogels. *Polymer Chemistry, 7*(44), 6752–6760. https://doi.org/10.1039/c6py01663d.

Ansteinsson, V., Kopperud, H. B., Morisbak, E., & Samuelsen, J. T. (2013). Cell toxicity of methacrylate monomers-The role of glutathione adduct formation. *Journal of Biomedical Materials Research - Part A, 101*(12), 3504–3510. https://doi.org/10.1002/jbm.a.34652.

Bae, H., Ahari, A. F., Shin, H., Nichol, J. W., Hutson, C. B., Masaeli, M., ... Khademhosseini, A. (2011). NIH public access. *Soft Matter, 7*(5), 1903–1911. https://doi.org/10.1039/C0SM00697A.

Bel Haaj, S., Magnin, A., Pétrier, C., & Boufi, S. (2013). Starch nanoparticles formation via high power ultrasonication. *Carbohydrate Polymers, 92*(2), 1625–1632. https://doi.org/10.1016/j.carbpol.2012.11.022.

Bel Haaj, S., Thielemans, W., Magnin, A., & Boufi, S. (2016). Starch nanocrystals and starch nanoparticles from waxy maize as nanoreinforcement: A comparative study. *Carbohydrate Polymers, 143*, 310–317. https://doi.org/10.1016/j.carbpol.2016.01.061.

Bloembergen, S., Vanegdom, E., Wildi, R., Mclennan, I. J., Lee, D. I., Klass, C. P., ... Leeuwen, J. V. A. N. (2010). Biolatex binders for paper and paperboard applications. *Jounral of Pulp and Paper Science, 36*(3–4), 1–11.

Dannert, C., Stokke, B. T., & Dias, R. S. (2019). Nanoparticle-hydrogel composites: From molecular interactions to macroscopic behavior. *Polymers, 11*(275), 1–35. https://doi.org/10.3390/polym11020275.

Elvira, C., Mano, J., San Román, J., & Reis, R. (2002). Starch-based biodegradable hydrogels with potential biomedical applications as drug delivery systems. *Biomaterials, 23*(9), 1955–1966. https://doi.org/10.1016/S0142-9612(01)00322-2.

Gaulding, J. C., Smith, M. H., Hyatt, J. S., Fernandez-Nieves, A., & Lyon, L. A. (2012). Reversible inter- and intra-microgel cross-linking using disulfides. *Macromolecules, 45*(1), 39–45. https://doi.org/10.1021/ma202282p.

Gilbert, T., Alsop, R. J., Babi, M., Moran-Mirabal, J., Rheinstädter, M. C., & Hoare, T. (2017). Nanostructure of fully injectable hydrazone-thiosuccinimide interpenetrating polymer network hydrogels assessed by small-angle neutron scattering and dSTORM single-molecule fluorescence microscopy. *ACS Applied Materials & Interfaces, 9*(48), 42179–42191. https://doi.org/10.1021/acsami.7b11637.

Grossutti, M., Bergmann, E., Baylis, B., & Dutcher, J. R. (2017). Equilibrium swelling, interstitial forces, and water structuring in Phytoglycogen nanoparticle films. *Langmuir, 33*(11), 2810–2816. https://doi.org/10.1021/acs.langmuir.7b00025.

Hammouda, B. (2004). *Scattering from fractal systems. In probing nanoscale structures. The SANS toolbox.* Retrieved fromNational Institute of Standards and Technologyhttps://www.ncnr.nist.gov/staff/hammouda/the_sans_toolbox.pdf.

Hammouda, B., Ho, D. L., & Kline, S. (2004). Insight into clustering in poly(ethylene oxide) solutions. *Macromolecules, 37*(18), 6932–6937. https://doi.org/10.1021/ma049623d.

Ip, A. C. F., Tsai, T. H., Khimji, I., Huang, P. J. J., & Liu, J. (2014). Degradable starch nanoparticle assisted ethanol precipitation of DNA. *Carbohydrate Polymers, 110*, 354–359. https://doi.org/10.1016/j.carbpol.2014.04.007.

Ismail, H., Irani, M., & Ahmad, Z. (2013). Starch-based hydrogels: Present status and applications. *International Journal of Polymeric Materials and Polymeric Biomaterials, 62*(7), 411–420. https://doi.org/10.1080/00914037.2012.719141.

Jackson, P. A., Widen, J. C., Harki, D. A., & Brummond, K. M. (2017). Covalent modifiers: A chemical perspective on the reactivity of α,β-Unsaturated carbonyls with thiols via Hetero-Michael addition reactions. *Journal of Medicinal Chemistry, 60*(3), 839–885. https://doi.org/10.1021/acs.jmedchem.6b00788.

Jia, S., Tang, Z., Guan, Y., & Zhang, Y. (2018). Order-disorder transition in doped microgel colloidal crystals and its application for optical sensing. *ACS Applied Materials & Interfaces, 10*(17), 14254–14258. https://doi.org/10.1021/acsami.8b01326.

Kheradvar, S. A., Nourmohammadi, J., Tabesh, H., & Bagheri, B. (2018). Starch nanoparticle as a vitamin E-TPGS carrier loaded in silk fibroin-poly(vinyl alcohol)-Aloe vera nanofibrous dressing. *Colloids and Surfaces B, Biointerfaces, 166*, 9–16. https://doi.org/10.1016/j.colsurfb.2018.03.004.

Kim, J.-Y., & Lim, S.-T. (2009). Preparation of nano-sized starch particles by complex formation with n-butanol. *Carbohydrate Polymers, 76*(1), 110–116. https://doi.org/10.1016/j.carbpol.2008.09.030.

Kim, H. Y., Han, J. A., Kweon, D. K., Park, J. D., & Lim, S. T. (2013). Effect of ultrasonic treatments on nanoparticle preparation of acid-hydrolyzed waxy maize starch. *Carbohydrate Polymers, 93*(2), 582–588. https://doi.org/10.1016/j.carbpol.2012.12.050.

Le Corre, D., & Angellier-Coussy, H. (2014). Preparation and application of starch nanoparticles for nanocomposites: A review. *Reactive & Functional Polymers, 85*, 97–120. https://doi.org/10.1016/j.reactfunctpolym.2014.09.020.

Li, S., Xia, Y., Qiu, Y., Chen, X., & Shi, S. (2018). Preparation and property of starch nanoparticles reinforced aldehyde–hydrazide covalently crosslinked PNIPAM hydrogels. *Journal of Applied Polymer Science, 135*(5), 1–13. https://doi.org/10.1002/app.45761.

Li, X., Qin, Y., Liu, C., Jiang, S., Xiong, L., & Sun, Q. (2016). Size-controlled starch nanoparticles prepared by self-assembly with different green surfactant: The effect of electrostatic repulsion or steric hindrance. *Food Chemistry, 199*, 356–363. https://doi.org/10.1016/j.foodchem.2015.12.037.

Li, Y., Liu, C., Tan, Y., Xu, K., Lu, C., & Wang, P. (2014). In situ hydrogel constructed by

starch-based nanoparticles via a Schiff base reaction. *Carbohydrate Polymers, 110*, 87–94. https://doi.org/10.1016/j.carbpol.2014.03.058.

Lima-Tenório, M. K., Tenório-Neto, E. T., Garcia, F. P., Nakamura, C. V., Guilherme, M. R., Muniz, E. C., ... Rubira, A. F. (2015). Hydrogel nanocomposite based on starch and Co-doped zinc ferrite nanoparticles that shows magnetic field-responsive drug release changes. *Journal of Molecular Liquids, 210*, 100–105. https://doi.org/10.1016/j.molliq.2014.11.027.

Lin, N., Huang, J., & Dufresne, A. (2012). Preparation, properties and applications of polysaccharide nanocrystals in advanced functional nanomaterials: A review. *Nanoscale, 4*(11), 3274–3294. https://doi.org/10.1039/c2nr30260h.

Liu, D., Wu, Q., Chen, H., & Chang, P. R. (2009). Transitional properties of starch colloid with particle size reduction from micro- to nanometer. *Journal of Colloid and Interface Science, 339*(1), 117–124. https://doi.org/10.1016/j.jcis.2009.07.035.

Ma, X., Jian, R., Chang, P. R., & Yu, J. (2008). Fabrication and characterization of citric acid-modified starch nanoparticles/plasticized-starch composites. *Biomacromolecules, 9*(11), 3314–3320. https://doi.org/10.1021/bm800987c.

Malafaya, P. B., Silva, G. A., & Reis, R. L. (2007). Natural – Origin polymers as carriers and scaffolds for biomolecules and cell delivery in tissue engineering applications. *Advanced Drug Delivery Reviews, 59*, 207–233. https://doi.org/10.1016/j.addr.2007.03.012.

Maurer, M. K., Condon, D. E., McKinney, H. E., & Kim, J. K. (2009). Photoresponsive interpenetrating network photonic crystal. *Proceedings of IEEE Sensors IEEE International Conference on Sensors,* 418–421. https://doi.org/10.1109/ICSENS.2009.5398256.

Nickels, J. D., Atkinson, J., Papp-Szabo, E., Stanley, C., Diallo, S. O., Perticaroli, S., ... Dutcher, J. R. (2016). Structure and hydration of highly-branched, Monodisperse phytoglycogen nanoparticles. *Biomacromolecules, 17*(3), 735–743. https://doi.org/10.1021/acs.biomac.5b01393.

Norisuye, T., Masui, N., Kida, Y., Ikuta, D., Kokufuta, E., Ito, S., ... Shibayama, M. (2002). Small angle neutron scattering studies on structural inhomogeneities in polymer gels: Irradiation cross-linked gels vs chemically cross-linked gels. *Polymer, 43*(19), 5289–5297. https://doi.org/10.1016/S0032-3861(02)00343-9.

Qiu, C., Yang, J., Ge, S., Chang, R., Xiong, L., & Sun, Q. (2016). Preparation and characterization of size-controlled starch nanoparticles based on short linear chains from debranched waxy corn starch. *LWT - Food Science and Technology, 74*, 303–310. https://doi.org/10.1016/j.lwt.2016.07.062.

Ramaraj, B., & Radhakrishnan, G. (1994). Modification of the dynamic swelling behaviour of poly(2-hydroxyethyl methacrylate) hydrogels in water through interpenetrating polymer networks (IPNs). *Polymer, 35*(10), 2167–2173. https://doi.org/10.1016/0032-3861(94)90245-3.

Saragih, G., Tamrin, T., Marpongahtun, Nasution, D. Y., & Abdillah (2018). Preparation of semi-IPN hydrogel from starch nanoparticles of magrove fruit and monomer acrylic acid using crosslinker N,N' methylene bisacrylamide. *AIP Conference Proceedings, 2049*. https://doi.org/10.1063/1.5082454.

Sharma, R. V., & Sharma, K. C. (1977). The structure factor and the transport properties of dense fluids having molecules with square well potential, a possible generalization. *Physica, 89*(1), 213–218. https://doi.org/10.1016/0378-4371(77)90151-0.

Sheeja, Manaf, O., Juraij, K., Sneha Sundaran, P., Ashitha, K., Aleena, L. S., ... Sujith, A. (2018). Polyethylene-g-starch nanoparticle biocomposites: Physicochemical properties and biodegradation studies. *Polymer Composites, 39*, E426–E440. https://doi.org/10.1002/pc.24503.

Sivakumaran, D., Maitland, D., & Hoare, T. (2011). Injectable microgel-hydrogel composites for prolonged small-molecule drug delivery. *Biomacromolecules, 12*(11), 4112–4120. https://doi.org/10.1021/bm201170h.

Stieger, M., Pedersen, J. S., Lindner, P., & Richtering, W. (2004). Are thermoresponsive microgels model systems for concentrated colloidal suspensions? A rheology and small-angle neutron scattering study. *Langmuir, 20*(17), 7283–7292. https://doi.org/10.1021/la049518x.

Sun, Q., Li, G., Dai, L., Ji, N., & Xiong, L. (2014). Green preparation and characterisation of waxy maize starch nanoparticles through enzymolysis and recrystallisation. *Food Chemistry, 162*, 223–228. https://doi.org/10.1016/j.foodchem.2014.04.068.

Tan, Y., Xu, K., Li, L., Liu, C., Song, C., & Wang, P. (2009). Fabrication of size-controlled starch-based nanospheres by nanoprecipitation. *ACS Applied Materials & Interfaces, 1*(4), 956–959. https://doi.org/10.1021/am900054f.

Thaiboonrod, S., Milani, A. H., & Saunders, B. R. (2014). Doubly crosslinked poly(vinyl amine) microgels: Hydrogels of covalently inter-linked cationic microgel particles. *Journal of Materials Chemistry B, 2*(1), 110–119. https://doi.org/10.1039/c3tb21579b.

Thoniyot, P., Tan, M. J., Karim, A. A., Young, D. J., & Loh, X. J. (2015). Nanoparticle–Hydrogel composites: Concept, design, and applications of these promising, multi-functional materials. *Advanced Science, 2*(1–2), 1–13. https://doi.org/10.1002/advs.201400010.

Tseitlin, A., Van Alstyne, D., & Bloembergen, S. (2012). US Patent Application US2012/0309246 A1.

Van Vlierberghe, S., Dubruel, P., & Schacht, E. (2011). Biopolymer-based hydrogels as scaffolds for tissue engineering applications: A review. *Biomacromolecules, 12*(5), 1387–1408. https://doi.org/10.1021/bm200083n.

Wang, K., Hasjim, J., Wu, A. C., Henry, R. J., & Gilbert, R. G. (2014). Variation in amylose fine structure of starches from different botanical sources. *Journal of Agricultural and Food Chemistry, 62*(19), 4443–4453. https://doi.org/10.1021/jf5011676.

Zhang, Z., Shan, H., Chen, L., He, C., Zhuang, X., & Chen, X. (2013). Synthesis of pH-responsive starch nanoparticles grafted poly (l-glutamic acid) for insulin controlled release. *European Polymer Journal, 49*(8), 2082–2091. https://doi.org/10.1016/j.eurpolymj.2013.04.032.

Zhu, J., Li, L., Chen, L., & Li, X. (2012). Study on supramolecular structural changes of ultrasonic treated potato starch granules. *Food Hydrocolloids, 29*(1), 116–122. https://doi.org/10.1016/j.foodhyd.2012.02.004.